

THE ROLE OF ROBUST ENGINEERING IN THE DESIGN OF A SCANNER FLEXURE

By Rodney Hoffman, Andy Singleton, and Gary R. Walker
ITT Industries Space Systems Division
Fort Wayne, Indiana

September 19, 2004

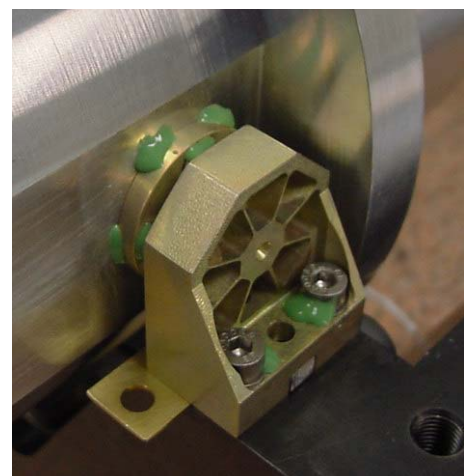
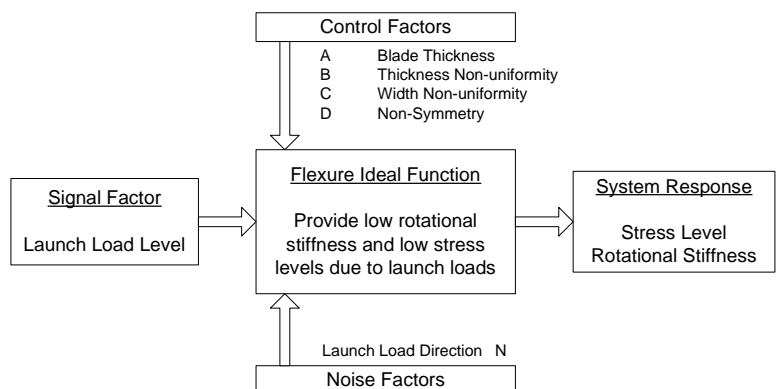
Abstract

Flexures are more reliable than bearings for long-life mechanisms with small magnitude motions. Typically made of metallic materials, a portion of the flexure is thinned dramatically to provide flexibility in the desired degree-of-freedom. When used in space-based remote sensors, the flexure also needs to survive launch-induced loads. The thinned sections act as stress risers in the part, which are susceptible to failure during launch vibration loading.

The flexure in a new infrared remote sensor catastrophically failed during a mass model vibration test. The flexure design was then revised using a L_9 orthogonal array with one noise factor. Two quality characteristics were evaluated, and the critical characteristic, peak stress level, was analyzed using a Smaller-the-Better signal-to-noise (S/N) ratio. A material study was conducted independently of the robust design experiment to validate the material selection for the application.

The design effort was complicated by the constraint to leave the flexure rotational stiffness unchanged while simultaneously improving the load carrying capability. If this requirement was ignored, the Taguchi experiment would have been quite successful, with a 98% improvement in the S/N ratio. However, this improved configuration was not feasible since it significantly affected the rotational stiffness. The primary benefit from the experiment was to identify a path for further design changes, and the relative importance of several control factors.

The design was completed within three days using one-at-a-time iterations of two additional control factors. The final flexure design has a S/N ratio as high as the experiment-recommended configuration without the change in rotational stiffness. Detailed structural analysis using a correlated model shows that all design requirements are satisfied, and the new flexure has been validated by a random vibration test.



INTRODUCTION

ITT's Space Systems Division (SSD) was formed on September 13, 2004 by the combination of the Aerospace/Communication Division space products with assets of Remote Sensing Systems acquired from Eastman Kodak. SSD is headquartered in Rochester, New York, and is a part of ITT Industries' Defense and Electronics segment. Other major operations are in Fort Wayne, Indiana (See Figure 1) and Clifton, New Jersey. SSD employs approximately 1,800 people and generated 2003 revenues of \$1.8 billion.

Space Systems' mission is to provide innovative imaging solutions to customers in Department of Defense, Intelligence, Space Science and Commercial Aerospace to help them visualize and understand critical events happening anywhere on earth, in the air, or in space. SSD's offering include Intelligence, Surveillance, and Reconnaissance Systems; Image Information Services; Software Technologies; GPS Navigation; Meteorological Imagers & Sounders; and Commercial Remote Sensing Systems & Space Science Systems.

ITT is under contract to develop the Cross-Track Infrared Sounder (CrIS) for the National Polar-orbiting Operational Environmental Satellite System (NPOESS) program. CrIS is an advanced instrument that will significantly improve weather forecasting and climate prediction by measuring vertical distributions of temperature, moisture, and pressure in the atmosphere. See Figure 2. It will help both short-term weather "nowcasting" and long-term forecasting. The sounding data is used to predict global and regional weather patterns, storm tracks, and precipitation. CrIS provides over one thousand spectral channels of information in the infrared at an improved horizontal spatial resolution, and measures temperature profiles with improved vertical resolution to an accuracy approaching one degree Kelvin.



Figure 1: SSD Facility in Fort Wayne, Indiana

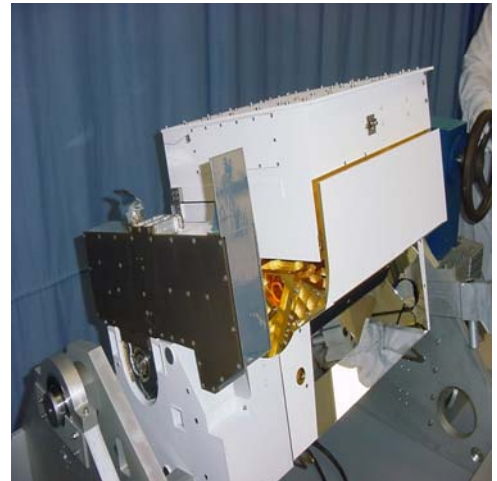


Figure 2: CrIS Instrument

BACKGROUND

The CrIS instrument will fly in a low-earth circular orbit. The primary function of the CrIS scanner module is to provide a stable line-of-sight during the each instrument dwell period of 0.167 second. The scanner compensates for spacecraft forward motion during each dwell to prevent a line-of-sight smear across the earth. The amount of scanner movement needed to compensate for spacecraft velocity motion is only 0.040 degrees, which is repeated 830 million times over the 7-year mission life. Bearings are unsuited for this application, and so a metallic flexure is used to provide the desired motion.

The original flexure was verified by structural analysis to have positive margins in the launch vibration environment. A vibration test of a scanner mass model was conducted to determine damping values for model correlation. Unfortunately, an anomaly was found during the test, and post-test inspection found several cracks in the flexure. See Figure 3.

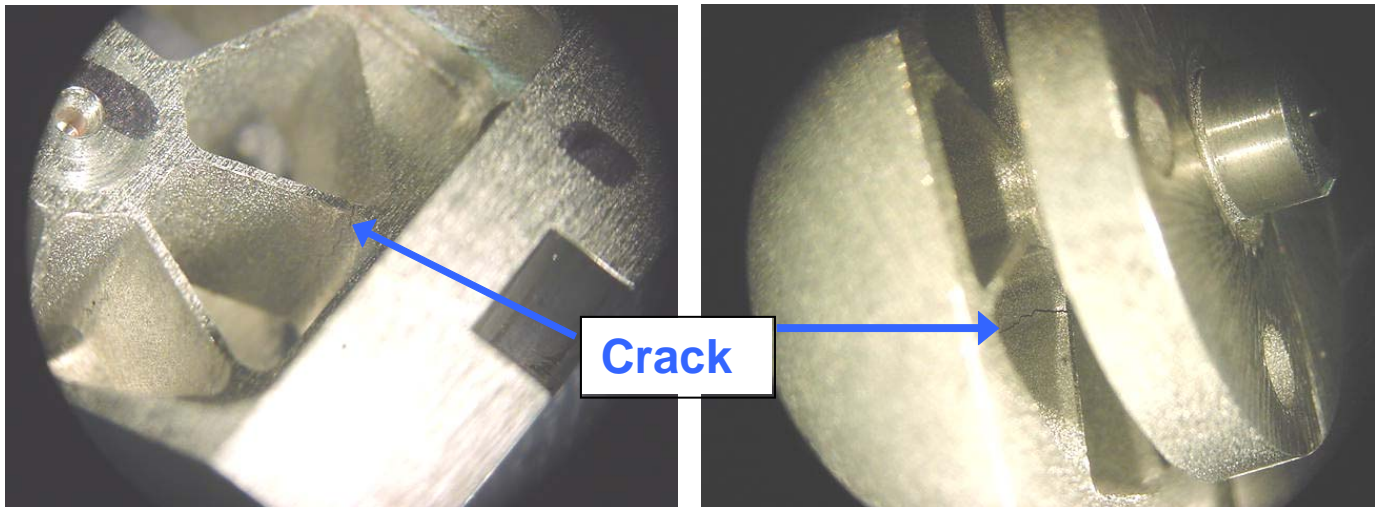


Figure 3: Post-test Fractures in Flexure

An extensive failure investigation revealed a number of contributing causes for the failure.

1. The finite element modeling technique did not accurately capture peak stress.
2. The analysis model did not match the as-built flexures. The blade thickness in the model was approximately 20% thicker than the design.
3. The mass model had a 650 Hz mode that was artificially low, and did not represent flight hardware. Post-test analysis shows that this mode is a high contributor to flexure stress.
4. During the fabrication process, tooling pressure induced an “hour glass” effect in the base of several blades. Local thickness due to this defect was 20% too thin. This defect was not found during the part inspection process.

Different element types were implemented in the structural model to accurately capture the peak flexure stress. The model was corrected to agree with the as-designed blade thickness. The modal correlation effort found that the scanner drive arm was not represented properly with a scaled spring element to simulate snubbing. Instead, the spring element was removed and the proper modal damping was introduced into the model.

Since the flexure is a critical part of the CrIS instrument design, it was also decided to increase the minimum design requirements, listed in Table 1, to prevent a re-occurrence of the failure on critical flight hardware.

Parameter	New Requirement	Previous Requirement
Yield Factor of Safety	2.00	1.25
Microyield	Positive margin with 1.0 factor of safety	Not applicable
Fatigue life (after two exposures to proto-qualification vibration)	At least 70% of life	At least 30% of life

Table 1: Enhanced Design Requirements

The combination of the structural model corrections plus the enhanced design requirements meant that the flexure design was no longer acceptable. Unfortunately for the program, the now-unacceptable flexure was already integrated into the flight pathfinder scanner. Moreover, this was a fully-functional unit, and the servo controller and driver electronics were already tailored to the rotational stiffness of this flexure.

An easy structural fix for the flexure would be to simply increase the blade thickness to the point that the enhanced requirements were satisfied. A side effect of this change is that the flexure rotational stiffness would increase significantly, resulting in the following impacts:

- Redesign of the scanner in-track servo controller
- Repeat of the plant characterization
- Redesign of the motor driver circuit to provide the increased current needed for the stiffer flexure
- Find other power savings within the scanner to offset the increase in in-track motor consumption

The program could not tolerate the cost or schedule impacts of the “easy” structural fix. The challenge facing the scanner design team was to satisfy the new structural requirements without changing the overall flexure stiffness.

OBJECTIVES

1. Keep the flexure rotational stiffness unchanged (within 10%)
2. Meet the enhanced flexure structural requirements
3. Any change to the flexure interface must involve the removal of material, since mating parts were already being fabricated for the scanner flight model
4. New flexure must be capable of being installed on the flight pathfinder scanner module
5. Flexure thermal conductance must be high to keep the motor on-orbit temperature within allowable limits

APPROACH

The original flexure design is shown in Figure 4. The flexure has eight thinned sections, or blades, that are rectangular in form. The rotational stiffness is defined by 4 factors, a) blade thickness, b) blade length, c) blade width, and d) material modulus of elasticity. Parameter changes were needed to allow additional load-carrying capability without affecting the stiffness. However, the most obvious changes to increase the load capacity would also significantly increase the stiffness. Therefore, the team focused on methods that would reduce the stress gradients within the part. Two basic ideas were competing within the design team:

- a) Reduce the stiffness of the two base blades to force the load to be more equally shared by the other six flexures. This would be accomplished by subtracting material from the base blades.
- b) Increase the load-carrying capacity of the two base blades, since the load wants to flow through them anyway. This would be accomplished by adding material to the base blades.

As one can see, the two approaches are diametrically opposed. Moreover, the stress gradient could also be reduced by making the blade geometry more complicated. This was a classical design problem, where the number of potential ideas was quite large, the schedule and funding to try them all was unavailable, and tracking all analysis data would be overwhelming.



Figure 4: Baseline Flexure Design

The team elected to follow a structured design approach by conducting a Parameter Design experiment. In parallel, a material trade study was performed to revisit the baseline material selection. The parameter diagram for this system is shown in Figure 5, along with the ideal function. The experiment factors are identified in Table 2, along with several other candidate factors that were rejected.

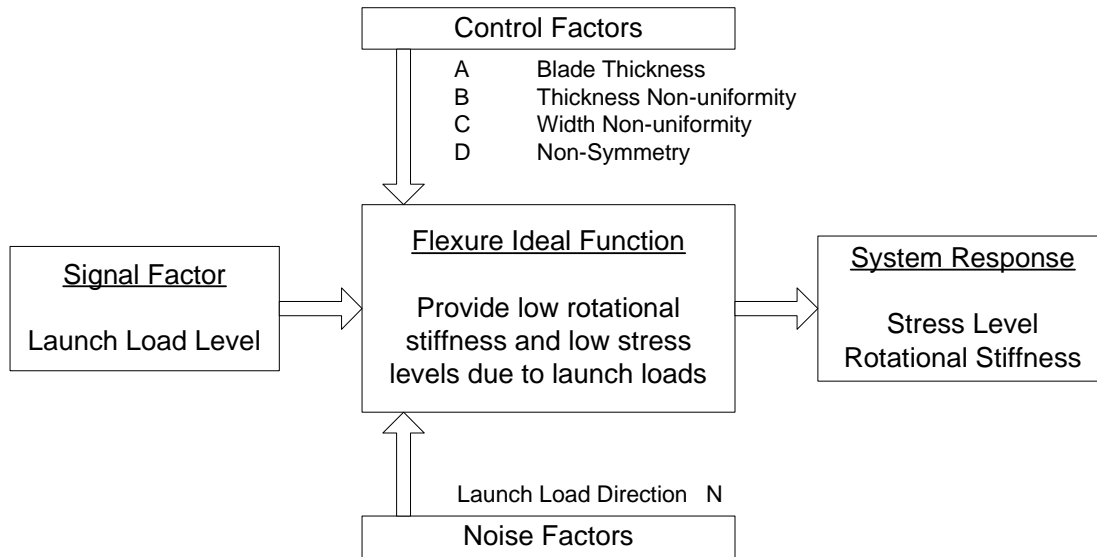


Figure 5: System Parameter Diagram and Ideal Function

Factor	Definition	Comment
Blade thickness	Thickness at base of blade	Included in experiment
Width taper	Ratio of width at blade center to width at base	
Thickness taper	Ratio of thickness at blade center to thickness at base	
Symmetry	Selective treatment of individual blades to increase load sharing	
Root radius	Radius at the root of each blade	<u>Not included</u> – effect is duplicated by thickness taper factor
Blade clocking	Alignment of blades with respect to the mounting surface	<u>Not included</u> – preliminary analysis revealed that these factors were ineffective
Number of blades	Baseline of eight	
Material	Leading candidates are 7075 aluminum and Beryllium-Copper	<u>Not included</u> – considered independently in a trade study. Alternate material effects could swamp any those of geometry changes, and any geometry improvement could be implemented using any material.
Blade center cutout	Remove material in the center section of each blade	<u>Not included</u> – adds risk to flexure fabrication and potential for significant stress risers

Table 2: Control Factors for Parameter Design Experiment

One noise factor was selected for the experiment, direction of applied vibration, since the structural requirements needed to be satisfied regardless of direction. Moreover, it was desired to have a solution that was not over-designed for any given direction, but yielded approximately equal performance. A L_9 experimental array was chosen for the control factors, and noise was treated with a three level full-factorial array. The full experiment array is shown in Figure 6. The factor levels were selected so that run #7 represented the baseline design.

Run	Control Factor				Noise: Direction of Applied Load		
	Blade Thickness (inch)	Thickness Taper	Width Taper	Blade Symmetry	X Axis	Y Axis	Z Axis
1	0.030	1.00	0.50	50%			
2	0.030	0.75	0.75	100%			
3	0.030	0.50	1.00	150%			
4	0.025	1.00	0.75	150%			
5	0.025	0.75	1.00	50%			
6	0.025	0.50	0.50	100%			
7	0.020	1.00	1.00	100%			
8	0.020	0.75	0.50	150%			
9	0.020	0.50	0.75	50%			

Level	Control Factor			
	Blade Thickness (inch)	Thickness Taper	Width Taper	Blade Symmetry
1	0.03	1.00	0.50	50%
2	0.025	0.75	0.75	100%
3	0.02	0.50	1.00	150%

Figure 6: Experimental Layout and Level Assignment

A process improvement was implemented to execute the analysis portion of the experiment. Each of the nine experiment runs was modeled in Pro/Engineer, and exported in IGES format. Finite element models were constructed using MSC Patran with MSC NASTRAN acting as the solver. A Patran based macro was created to reduce the finite element modeling cycle time on each experiment. The macro automatically imported the geometry, generated a solid TET10 mesh, and applied loads, constraints and material data. This automation technique reduced the cycle time to evaluate each experiment to 9 minutes from the original analysis time of 45 minutes.

Fidelity of the finite element models was increased by using solid TET10 elements to capture design details in varying cross sections, such as fillets, of the blades. This was a great improvement over earlier modeling techniques where constant thickness shells were used to model the flexure blades. For analysis solutions, such as random, that do not directly support the solid element type, a thin 2-D shell skin was applied to the exposed solid element face to extract surface stresses.

The actual loading environment is random vibration due to the launch vehicle dynamic characteristics during rocket firing. Performing a random vibration analysis is computationally-intensive, and would have delayed the experiment completion. Another process improvement implemented for this experiment was to conduct a static loading analysis instead of random vibration. While the magnitude of the resulting stress level would not be meaningful, the relative flexure performance for each of the experiments should be about the same for both analysis methods. A unit load was used since we were interested in relative changes only.

For each experimental run, the peak stress anywhere within the flexure was captured. The signal-to-noise equation is listed below, where σ_i is the peak stress in the i-th direction.

$$S / N = -10 \log \left(\frac{\sigma_x^2 + \sigma_y^2 + \sigma_z^2}{3} \right)$$

RESULTS

Material Study - A number of alternate materials were considered to replace the baseline 7075-T7351 aluminum. In order to minimize the rotational stiffness while still being capable of carrying high loads, it was soon realized that the critical parameter is the ratio of the Yield Strength to the Young's Modulus of Elasticity. The former is a measure of the material's load-carrying capability, while the latter is a measure of the material stiffness. The thermal conductivity is of secondary importance, as only a moderate level of performance would be adequate.

These parameters are shown in Table 3, where the materials are listed in order of descending values of the critical parameter. Three materials score better than the baseline. The best material, titanium, was not selected due to the extremely poor thermal conductivity. The next material, beryllium copper, was rejected because very thin blade sections would be required due to the high modulus, which is a fabrication risk. Stainless steel was rejected due to its low thermal conductivity. Thus the baseline material, 7075-T7351 aluminum, was found to be an appropriate choice for the flexure application.

Material	Yield Strength (ksi)	Young's Modulus (10 ⁶ psi)	Yield Strength / Modulus	Thermal Conductivity (BTU/hr ft F)
Titanium, Ti-6Al-4V	160	17	9.7	4
Beryllium Copper, C17200	125	19	6.8	69
Stainless Steel, 17-4PH	183	29	6.3	10
Aluminum, 7075-T7351	57	10	5.7	70
Magnesium, AZ31	30	7	4.6	44
Copper-Tungsten, Thermkon 62	116	37	3.1	91
Copper-Moly, Thermkon 65M	95	36	2.6	78
Molybdenum, TZM	115	46	2.5	84

← Baseline material

Table 3: Material Trade Study Results

Parameter Design – The correlated scanner structural model was utilized to generate the experiment data. A unit static load was applied to the model and the peak Von Mises stress captured. The load direction was varied to fill the noise factor outer array. The rotational stiffness was found by imposing a static torque and recovering the amount of rotation. The stiffness is then the ratio of the two. A static thermal run was used to recover the flexure conductivity. The raw data from all of runs is in Table 4.

Run	Stress VonMises (Mpa)			Stiffness (N-m/rad)	Conductance (W/K)
	X Axis	Y Axis	Z Axis		
1	0.593	0.233	0.919	281	0.28
2	0.457	0.171	0.592	376	0.34
3	0.452	0.156	0.5	452	0.37
4	0.361	0.139	0.414	380	0.36
5	0.516	0.191	0.782	237	0.31
6	0.998	0.294	1.05	159	0.25
7	0.567	0.195	0.673	174	0.32
8	0.832	0.266	0.798	169	0.27
9	0.928	0.298	1.42	90	0.28

Table 4: Parameter Design Experiment Results

ANALYSIS

An analysis was conducted on the peak stress values to determine a) the factor settings that would make the flexure able to carry loads equally-well in any direction, and b) the means to minimize the stress level. The peak stress levels are listed in Table 5, along with the resulting S/N ratio. The level-average graph is shown in Figure 7.

Run	Stress VonMises (Mpa)			S/N Ratio
	X Axis	Y Axis	Z Axis	
1	0.593	0.233	0.919	3.80
2	0.457	0.171	0.592	7.07
3	0.452	0.156	0.5	7.97
4	0.361	0.139	0.414	9.71
5	0.516	0.191	0.782	5.16
6	0.998	0.294	1.05	1.38
7	0.567	0.195	0.673	5.67
8	0.832	0.266	0.798	3.31
9	0.928	0.298	1.42	0.05

Table 5: Signal-to-Noise Experiment Values

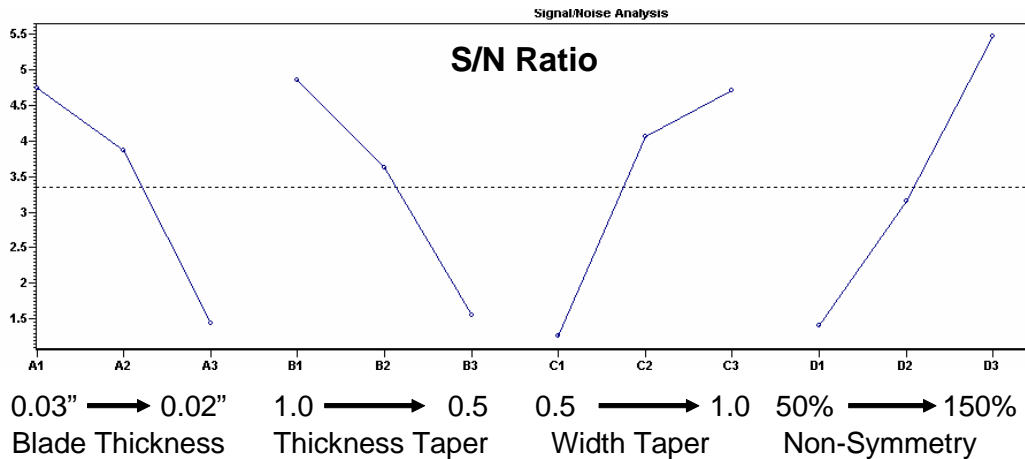


Figure 7: Signal-to-Noise Level Average Graph

CONFIRMATION

It was found that adding material to the flexure not only lowered the peak stress, but also made the flexure less sensitive to the direction of applied force. Unfortunately, this approach was not possible, as it would have nearly doubled the rotational stiffness. Another approach was to select factor levels that kept the stiffness essentially unchanged, however, this allowed only a marginal improvement in stress S/N.

Keeping the stiffness within 10% of the original value was a critical design parameter, and so the team went back to the drawing board. Two additional control factors were found that allowed an increase in the stress S/N ratio without affecting the rotational stiffness. The data summary for these configurations is listed in Table 6.

Configuration	S/N Ratio	Stiffness (N-m/rad)
Baseline (pre-experiment)	5.67	174
Confirmation: Minimum Stress	11.2	497
Confirmation: Unchanged Stiffness	6.4	224
Final Design	11.1	172

Table 6: Flexure Configuration Data Summary

The experimental method was verified by performing a process estimate within ANOVA, and comparing it to an independent structural model run. This was performed for both the peak stress value, and the rotational stiffness. Since the stress values from all three axes were in the ANOVA data set used to generate the process estimate, the average stress from NASTRAN was utilized. The correlation is satisfactory since the error was within the predicted confidence interval. Final confirmation results are shown in Table 7.

	Stress VonMises (Mpa)				Stiffness (N-m/rad)
	X Axis	Y Axis	Z Axis	Average	
NASTRAN Model	0.57	0.19	0.57	0.44	224
ANOVA Process Estimate	-	-	-	0.42	254
Error	-	-	-	6.6%	13.5%

Table 7: Experiment Confirmation Results

CONCLUSIONS

- The experiment was very successful. Its primary benefit was to focus the team on a design direction that enhances the cross-section of the two base blades, rather than load spreading among the eight flexures.
- The primary shortcoming of the experiment is that all initial control factors moved both the stress S/N and the rotational stiffness in the same direction. See Figure 8. It is desired to maximize the S/N ratio while simultaneously maintaining the stiffness at 174 N-m/rad.

- Two control factors were overlooked when setting up the initial experiment. These factors, found after the experiment had focused the team, allowed an increase in the S/N ratio without an attendant stiffness increase. See Figure 9. A lesson-learned is that a follow-up experiment, including all six control factors, may have led to even better performance.
- The process improvements associated with the experiment analysis methods were very successful. Static loading was employed to greatly reduce the experiment cost and duration, and performance under random vibration conditions was checked only after an improved flexure configuration was found. The automated Pro/Engineer to NASTRAN model process reduced analysis cycle time by a factor of 5.
- Solid modeling software, Pro/Engineer, was used to generate each of the unique experiment physical configurations. This approach was very effective not only to improve the efficiency of structural model mesh generation, but also to reduce the risk of modeling errors. The Pro/Engineer model was constructed to be parameter-driven, so that only a handful of model dimensions needed to be changed for each experiment run.
- The original flexure material, 7075-T7351 aluminum, was the best material due to the competing material requirements for high strength, low stiffness, and high-to-moderate thermal conductance.
- The new flexure meets all of the enhanced structural requirements. The rotational stiffness of the flexure is within 98.8% of the target value, thus preserving the program investment in the servo control and electrical design.
- The new flexure has been validated by two random vibration tests, the mass model (see Figure 10) and the flight pathfinder scanner. Both tests were fully successful, thus allowing the flight scanner to proceed with low risk.

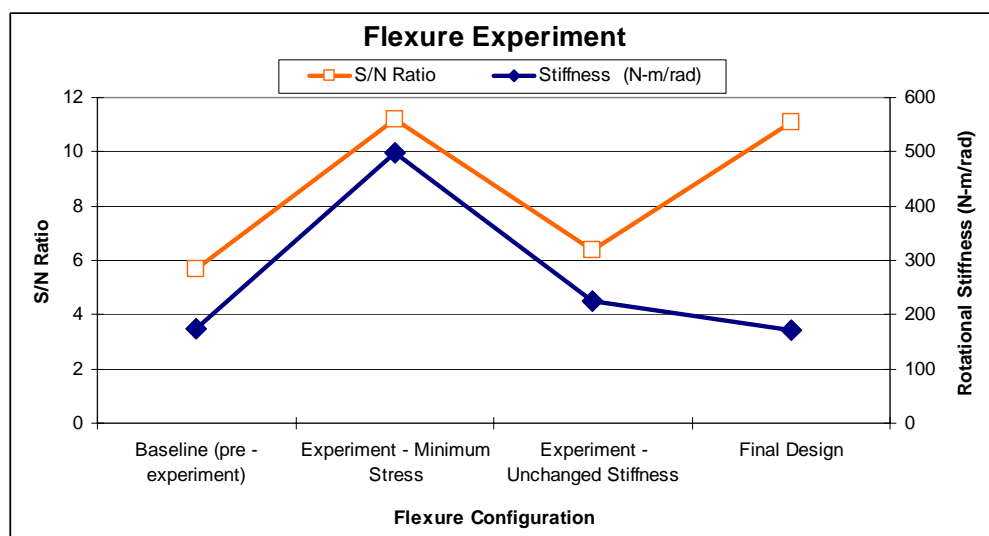


Figure 8: Final Design Features 2X Improvement in S/N without Affecting Stiffness

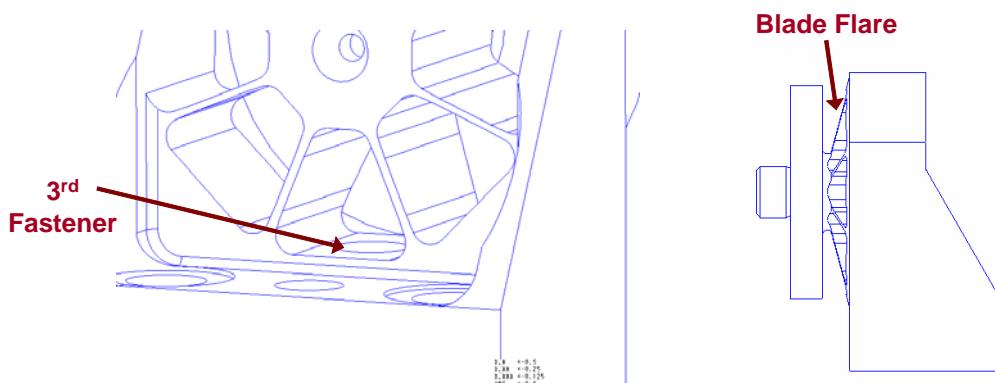


Figure 9: Post-Experiment Control Factors

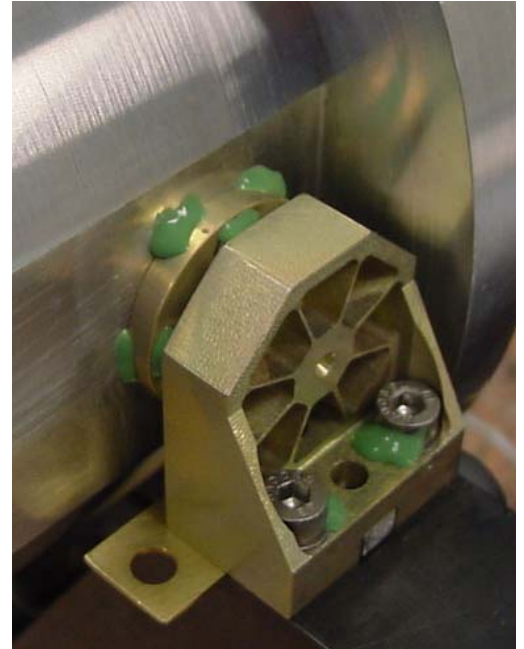
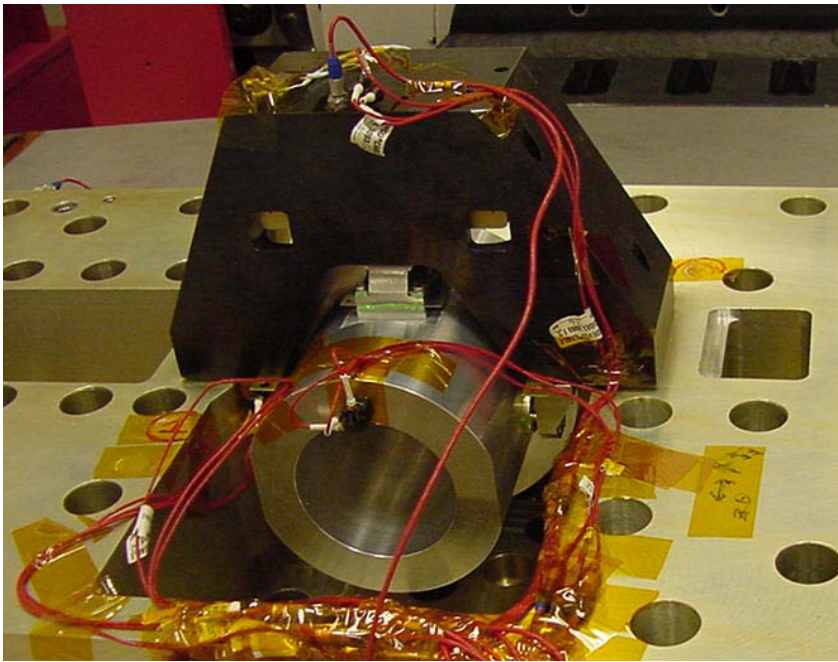


Figure 10: Mass Mockup Vibration Test Validates Final Flexure Design